

NASA TECHNICAL NOTE



NASA TN D-4465

c. 1

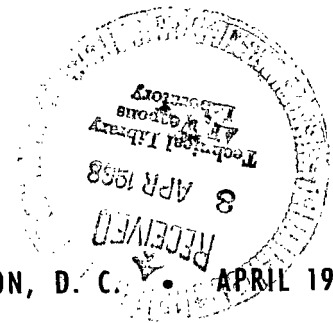
NASA TN D-4465



LOAN COPY: RETURN TO  
AFWL (WLIL-2)  
KIRTLAND AFB, N MEX

# AN INVESTIGATION OF EXTREMELY FLEXIBLE LIFTING ROTORS

*by Matthew M. Winston*  
*Langley Research Center*  
*Langley Station, Hampton, Va.*



NATIONAL AERONAUTICS AND SPACE ADMINISTRATION • WASHINGTON, D. C. • APRIL 1968



AN INVESTIGATION OF EXTREMELY FLEXIBLE LIFTING ROTORS

By Matthew M. Winston

Langley Research Center  
Langley Station, Hampton, Va.

NATIONAL AERONAUTICS AND SPACE ADMINISTRATION

---

For sale by the Clearinghouse for Federal Scientific and Technical Information  
Springfield, Virginia 22151 - CFSTI price \$3.00

# AN INVESTIGATION OF EXTREMELY FLEXIBLE LIFTING ROTORS

By Matthew M. Winston  
Langley Research Center

## SUMMARY

This investigation includes analytical and experimental studies of rotors with very low structural stiffness and single-surface, deformable airfoils. The analytical study focused on the planform and tip-mass requirements necessary to prevent luffing (fabric instability) of a completely flexible blade and included consideration of the aeroelastic characteristics of flexible blades having chordwise stiffeners spaced along the blade. The experimental investigation focused on determining the hovering characteristics of a 30-foot- (9.144-meter-) diameter flexible rotor. The results of the analytical study indicate that very careful planform design and judicious choice of tip mass are required to prevent luffing on a completely flexible blade. Tip-mass requirements with the attendant increase in overall rotor weight indicate that large rotors of this type are not assured the performance benefits of low disk loadings that were initially expected. Although partial stiffening of the blade chord makes planform and tip-mass design requirements less critical, both types of flexible rotors may operate at disk loadings higher than initially expected, since rotor size-weight relationships may be dictated by requirements for aeroelastic stability. The experimental study indicates that low hovering efficiencies and high power consumption resulted from blade deformations and excessive twist; however, the aerodynamically-induced camber developed during operation provided high mean lift coefficients.

## INTRODUCTION

Recent interest in extremely flexible rotors stems from several distinct advantages which they are believed to possess over conventional rotors. For the very large load-lifting helicopters being considered for future use, the rotor size required and the attendant weights of large conventional rotors pose considerable storage and structural problems. The problems of both size and weight could become less severe with an extremely flexible lightweight rotor which could be retracted into a small package when not in use. Also, large lightweight rotors could operate at lower disk loadings and thereby accrue significant performance gains over the heavier types. In addition, interest in flexible rotors for convertible aircraft and for recovery systems has been expressed.

The present conception of the flexible rotor involves a number of new design considerations and leads to both old and new problem areas. The low stiffness of these rotors suggests that classical aeroelastic problems, such as flutter, may require attention. For those rotor blades with fabric lifting surfaces, the primary new problem is expected to be a type of fabric instability known as luffing.

In this paper, the general characteristics of flexible rotors are discussed, and a planform design method for nonluffing rotor blades is outlined. Also included herein is an elementary analysis of the factors involved in the aeroelastic stability of extremely flexible rotors. Some experimental results from a fully flexible rotor hovering investigation are presented and compared with results from a similar investigation of a conventional rotor.

### SYMBOLS

The physical quantities defined in this section are given in both U.S. Customary Units and the International System of Units (SI). Factors relating the two systems are given in reference 1.

A	distance from airfoil leading edge to aerodynamic center, ft (meters)
a	slope of section lift coefficient per unit blade span as a function of angle of attack, per degree or per radian
B	distance from airfoil leading edge to elastic axis, ft (meters)
b	number of blades
$\bar{c}$	chordwise distance from planform baseline to leading or trailing edge, ft (meters)
c	airfoil chord, ft (meters)
$C_L$	airfoil lift coefficient
$C_Q$	torque coefficient, $\text{Torque}/\pi R^2 \rho (\Omega R)^2 R$
$C_T$	thrust coefficient, $\text{Thrust}/\pi R^2 \rho (\Omega R)^2$
$c_0$	minimum chord, ft (meters)

d	distance measured along airfoil chord, ft (meters)
F	chordwise component of centrifugal force, lbf (newtons)
G	distance from airfoil leading edge to center of gravity, ft (meters)
H	horizontal component of centrifugal force at minimum chord point, lbf (newtons)
I <sub>G</sub>	mass moment of inertia of blade section and surrounding air about center of gravity, slugs-ft <sup>2</sup> (kilograms-meter <sup>2</sup> )
K <sub>t</sub>	tension constant in equation of rotor planform
K <sub>θ</sub>	torsional spring constant, lbf-ft/radian (newton-meters/radian)
K <sub>y</sub>	flapwise spring constant, lbf/ft (newtons/meter)
L	airfoil lift per unit blade span, lbf/ft (newtons/meter)
M <sub>θ</sub>	torsional restoring moment, lbf-ft (newton-meters)
M <sub>O</sub>	aerodynamic moment about airfoil half-chord point, lbf-ft (newton-meters)
m	mass, slugs (kilograms)
$\bar{m}$	portion of tip-body mass supported at leading or trailing edge, slugs (kilograms)
m <sub>tip</sub>	total mass of tip body, slugs (kilograms)
q	dynamic pressure, $\frac{1}{2} \rho V^2$ , lbf/ft <sup>2</sup> (newtons/meter <sup>2</sup> )
R	radius to rotor blade tip, ft (meters)
r	radius to any blade station, ft (meters)
r <sub>O</sub>	radius to minimum chord point, ft (meters)

S	component of centrifugal force along edge member, lbf (newtons)
t	chordwise tension per unit blade radius, lbf/ft (newtons/meter)
V	velocity at rotor blade section, ft/sec (meters/second)
x	ratio of any radius to tip radius, $r/R$
$x_0$	ratio of radius to minimum chord to tip radius, $r_0/R$
y	vertical distance, ft (meters)
$\alpha$	angle of attack, radians
$\beta$	angle between the blade span axis and a plane perpendicular to the axis of rotation (nonarticulated rotor assumed), radians
$\gamma$	angle between baseline of rotor planform and line joining center of rotation to tip body attachment point at leading or trailing edge, radians
$\epsilon$	angle between spanwise and edgewise components of centrifugal force at minimum chord point, $\cos^{-1} \frac{H}{S}$ , radians
$\theta$	angle between blade chord line and plane perpendicular to axis of rotation, radians
$\rho$	air density, slugs/ft <sup>3</sup> (kilograms/meters <sup>3</sup> )
$\sigma$	rotor solidity, $bc/\pi R$
$\sigma_{tip}$	local solidity at blade tip, $c_{tip}/\pi R$
$\Omega$	rotational velocity, radians/second

Subscripts:

tip	pertains to conditions at blade tip or to tip body
y	pertains to vertical distance, motion, or force

- le            pertains to leading edge
- te            pertains to trailing edge
- 0            pertains to conditions at blade root

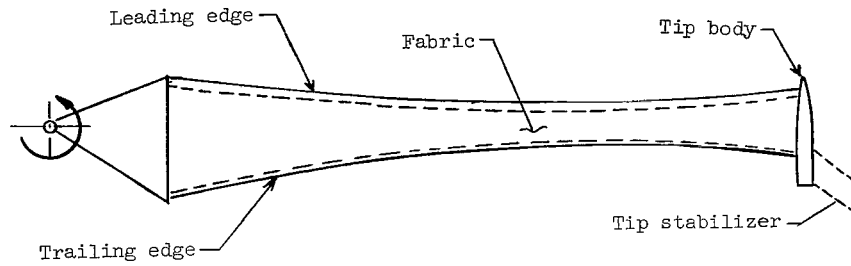
## ANALYTICAL INVESTIGATION

### General Description of the Flexible Rotor

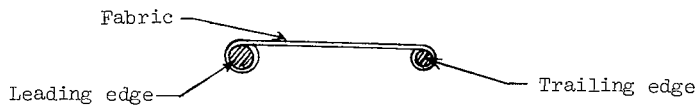
The flexible rotor blade, as presently conceived, is composed of a fabric airfoil surface fastened to cables or very flexible rods at the leading and trailing edges. The edge members are designed to carry the centrifugal forces generated by a concentrated mass at the blade tip. In some designs, centrifugal stiffening effects provide the only resistance to flapwise bending, in-plane bending, chordwise blade deformation, and torsion. (See fig. 1(a).) With the fully flexible rotor, the airfoil section properties (camber and camber distribution) are dependent upon the operating conditions. In other designs, resistance to flapwise bending and torsion is also provided by centrifugal forces; however, the chordwise rigidity is supplied by stiffening members spaced along the blade span. (See fig. 1(b).) In either design, the extremely flexible rotor, as presently conceived, has essentially no static flapwise nor torsional stiffness; and centrifugal forces determine its behavior to a large degree.

### Luffing

One outstanding problem peculiar to the fully flexible rotor blade is luffing. Luffing is characterized by rapid reversals of camber and is believed to be a result of positive pressures on the convex surface of the fabric. Luffing causes rapid variations in thrust and pitching moment which in turn cause undesirable rotor vibrations. Luffing can be considered as a "low-pitch" phenomenon because it usually can be relieved by increasing the blade-pitch angle. For this type of blade, however, a pitch input at the blade root does not provide an equal increment of pitch angle at every blade radius. The angle at which the tip and outboard blade sections operate is primarily determined by the centrifugal restoring moments generated by the tip body and the aerodynamic moments produced by the tip stabilizer when one is used. Since the blade is torsionally very "soft," a change in pitch at the root primarily causes a change in blade twist. Thus the root pitch angle required to bring all blade sections above the minimum nonluffing pitch angle may be large; and since the minimum local angles required at a section increase with local velocity, inboard blade sections may stall before luffing is relieved at the higher velocities near the tip. The approximate shape of the operating envelope for a luffing rotor is

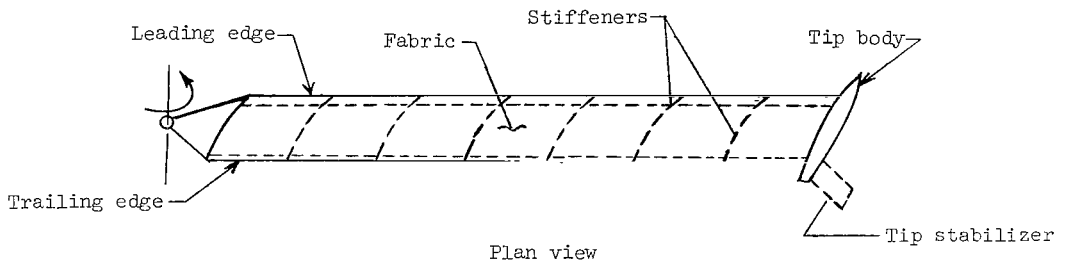


Plan view

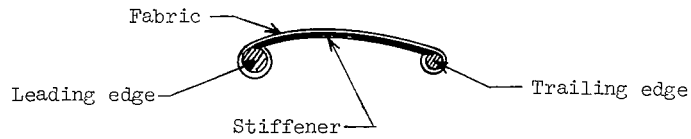


Cross section

(a) Fully flexible blade.



Plan view



Cross section through a stiffener

(b) Flexible blade with stiffeners.

Figure 1.- Typical flexible rotor blades.

shown in figure 2. Further studies are necessary to determine the major influences of rotor operating parameters on these boundaries and to define other general problems of this type of rotor.

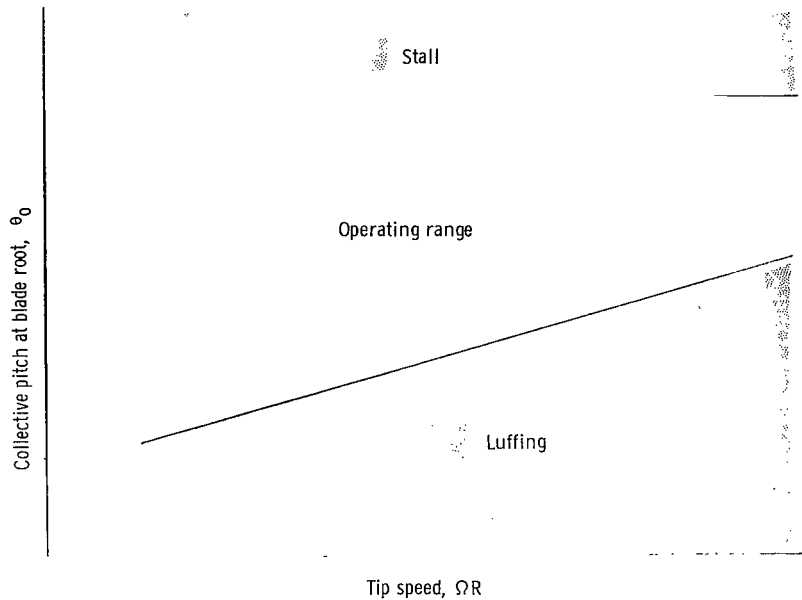


Figure 2.- General shape of operating envelope for luffing rotor.

### Design of a Nonluffing Blade

Because luffing imposes limitations on the performance of flexible airfoils, much attention has been given to this problem. The analysis in reference 2 concludes that to maintain a stable single curvature on an extremely flexible lifting surface down to very small angles of attack, a certain minimum ratio of chordwise tension to aerodynamic load per unit span must exist at every point on the surface. For a fully flexible rotor, the chordwise tension is produced by the centrifugal forces from the tip body acting on the curved leading and trailing edges. The aerodynamic load is the product of the dynamic pressure and the blade chord dimension. Reference 2 defines the luffing parameter as  $t/qc$  and indicates that if  $t/qc$  is maintained greater than 1.73, a nonluffing rotor blade results. When this ratio is used as a design criterion, it is possible to design a hovering rotor blade for which a minimum  $t/qc$  is always maintained or exceeded. The required inputs are compatible with rotor blade design conventions, and solutions require only simple mathematical techniques.

Analysis. - Figure 3(a) shows a rotor planform of radius  $R$ , minimum chord  $c_o$ , tip chord  $c_{tip}$ , radius to the minimum chord  $r_o$ , and tip mass  $m_{tip}$ . The leading- and trailing-edge chord dimensions  $\bar{c}_{le}$  and  $\bar{c}_{te}$  are measured from a baseline which is determined by the tip center-of-gravity location as is shown later. The leading and trailing portions of the blade chord are computed separately and added to obtain the total chord at a given radial station. Since the procedure for each edge is identical, only the general equation for one edge is developed herein.

At the minimum chord point on the leading or trailing edge of the blade at radius  $r_o$ , the forces on the fabric are as shown in the free-body sketch of figure 3(b). In figure 3(b), the origin of the coordinates is on the baseline at  $r_o$  so that the chordwise tension at any point  $r$  can be written as the product of the unit tension and the radial distance from the origin or  $t(r - r_o)$ . From the resulting force triangle in figure 3(c),

$$\tan \epsilon = \frac{d\bar{c}}{dr} = \frac{t(r - r_o)}{H} \quad (1a)$$

Since the nonluffing criterion is that the ratio  $t/qc$  must be equal to or greater than a constant  $K_t$ , the unit tension must be  $K_t q \bar{c}$ . The dynamic pressure at a given radial blade station in hover is  $\frac{1}{2} \rho (\Omega r)^2$ . Therefore equation (1a) can be expressed as:

$$\frac{d\bar{c}}{dr} = \frac{\frac{1}{2} K_t \rho (\Omega r)^2 (r - r_o) \bar{c}}{H} \quad (1b)$$

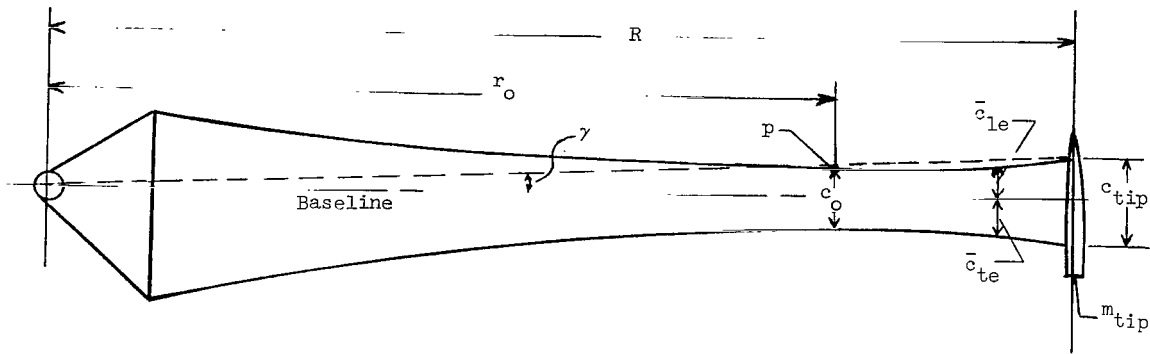
and

$$H = \sqrt{S^2 - [t(r - r_o)]^2} \quad (2a)$$

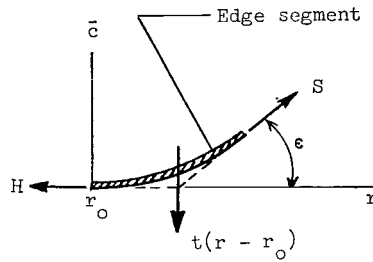
For an evaluation of  $H$ , consideration of conditions at the blade tip is convenient. If the angle  $\gamma$  in figure 3(a) is considered to be small,  $S \approx \bar{m} \Omega^2 R$  and  $H$  can be expressed as:

$$H = \sqrt{(\bar{m} \Omega^2 R)^2 - \left[ \frac{1}{2} K_t \rho (\Omega R)^2 \bar{c}_{tip} (R - r_o) \right]^2} \quad (2b)$$

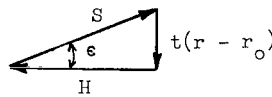
where  $\bar{m}$  is the fraction of the tip mass supported by the leading or trailing edge as determined from the design tip chordwise center of gravity. Substituting equation (2b) into equation (1b) gives:



(a) Rotor planform.



(b) Forces on edge segment at point p.



(c) Force triangle at point p.

Figure 3.- Forces on fully flexible rotor.

$$\frac{d\bar{c}}{dr} = \frac{K_t \rho}{2R} \left\{ \frac{r^2(r - r_o)\bar{c}}{\sqrt{\bar{m}^2 - \left[ \frac{1}{2} K_t \rho R \bar{c}_{tip} (R - r_o) \right]^2}} \right\} \quad (3a)$$

which can be written:

$$\frac{d\bar{c}}{\bar{c}} = \frac{K_t \rho}{2R} \left\{ \frac{(r^3 - r^2 r_o) dr}{\sqrt{\bar{m}^2 - \left[ \frac{1}{2} K_t \rho R \bar{c}_{tip} (R - r_o) \right]^2}} \right\} \quad (3b)$$

Since the denominator on the right side of equation (3b) is a constant, integration of both sides gives:

$$\log_e \bar{c} = \frac{K_t \rho}{2R} \left\{ \frac{\frac{r^4}{4} - \frac{r^3}{3} r_o}{\sqrt{\bar{m}^2 - \left[ \frac{1}{2} K_t \rho R \bar{c}_{tip} (R - r_o) \right]^2}} \right\} + \log_e C_i \quad (4)$$

where  $C_i$  is a constant of integration. To evaluate  $C_i$  consider that  $\bar{c} = \bar{c}_{tip}$  when  $r = R$ . From this condition and letting  $x = r/R$  and  $x_o = r_o/R$ , equation (4) can be expressed as:

$$\log_e \bar{c} = \frac{K_t \rho R^3}{24} \left\{ \frac{3(x^4 - 1) + 4x_o(1 - x^3)}{\sqrt{\bar{m}^2 - \left[ \frac{1}{2} K_t \rho R^2 \bar{c}_{tip} (1 - x_o) \right]^2}} \right\} + \log_e \bar{c}_{tip} \quad (5)$$

Equation (5) (the rotor planform equation) can then be used to solve for the blade chord as a function of radius. First however, the value of the blade chord at the tip must be determined. Examination of equation (5) indicates that the equation becomes discontinuous when

$$\bar{m} = \frac{1}{2} K_t \rho R^2 \bar{c}_{tip} (1 - x_o) \quad (6a)$$

This value of tip mass is the minimum tip mass for which the nonluffing planform equation is applicable. Since equation (6a) applies only to the leading or trailing portion of the blade, the minimum tip mass for the entire blade is:

$$m_{tip} = \frac{1}{2} K_t \rho R^2 (1 - x_o) c_{tip} \quad (6b)$$

where  $c_{tip}$  is the full chord at the blade tip. The blade local solidity at the tip is defined as  $\sigma_{tip} = c_{tip}/\pi R$ . Substituting this local solidity into equation (6b) yields the minimum tip mass as

$$m_{tip} = 1.57 K_t \rho R^3 (1 - x_o) \sigma_{tip} \quad (6c)$$

From a chosen blade radius and local tip solidity  $\sigma_{tip}$  the tip chord  $c_{tip}$  can be determined. From equation (6c) the minimum tip mass  $m_{tip}$  can be found. Then from the desired position of the tip-mass center of gravity, the leading and trailing portions of tip mass and tip chord can be computed. These values may then be used in equation (5) in which the only remaining unknown is the local chord  $c$ .

Results.- The foregoing analysis provides a method of computing nonluffing planforms. From the design variables  $K_t$ ,  $R$ ,  $x_o$ , and  $\sigma_{tip}$  a wide choice of nonluffing flexible blade planforms can be designed. The limitation imposed by this method is that the required tip mass for a given set of these parameters is a function of  $R^3$  (see eq. (6c)), and therefore, for large diameter rotors, the required tip masses can become quite heavy. Consequently, large rotors will require heavier leading- and trailing-edge members, heavier fabrics, and more massive blade retention hardware; all of which contribute to increased overall weight. Although disk loading decreases as  $R^2$ , tip-mass requirements with the accompanying weight requirements indicate that large rotors of this type are not assured the performance benefits of low disk loadings as initially expected. A numerical example which employs the preceding planform approach is given in the appendix. A sample of a nonluffing planform from the appended example is given in figure 4.

#### Flexible Blade With Chordwise Stiffeners

Some of the problems of the fully flexible rotor blade can be alleviated by providing fixed chordwise stiffening members as shown in figure 1(b). These members may be made to form a desired airfoil profile, and a spanwise arrangement may be chosen to provide a blade planform according to performance considerations. Since the airfoil camber cannot reverse, luffing should not be a problem; although some study is required to determine the optimum spacing of stiffeners in relation to other blade parameters to minimize airload-induced deformations of the unsupported blade sections. Since chord-line stiffness is not dependent upon centrifugal force, the tip-mass requirements will not be as great, and the goal of low disk loading for large rotors may be more readily attained. Although no information is available on the effects of tip body mass and mass distribution relative to spanwise twist and thrust distribution, it is expected that this type of rotor will permit simpler analyses of these effects in comparison to the fully flexible type.

The question of rotor aeroelastic characteristics is much the same, however, for both the fully flexible and the stiffened chord blades since both types derive essentially all of their flapwise and torsional rigidity from centrifugal forces. The next section of this paper gives an elementary aeroelastic analysis of a hovering flexible rotor.

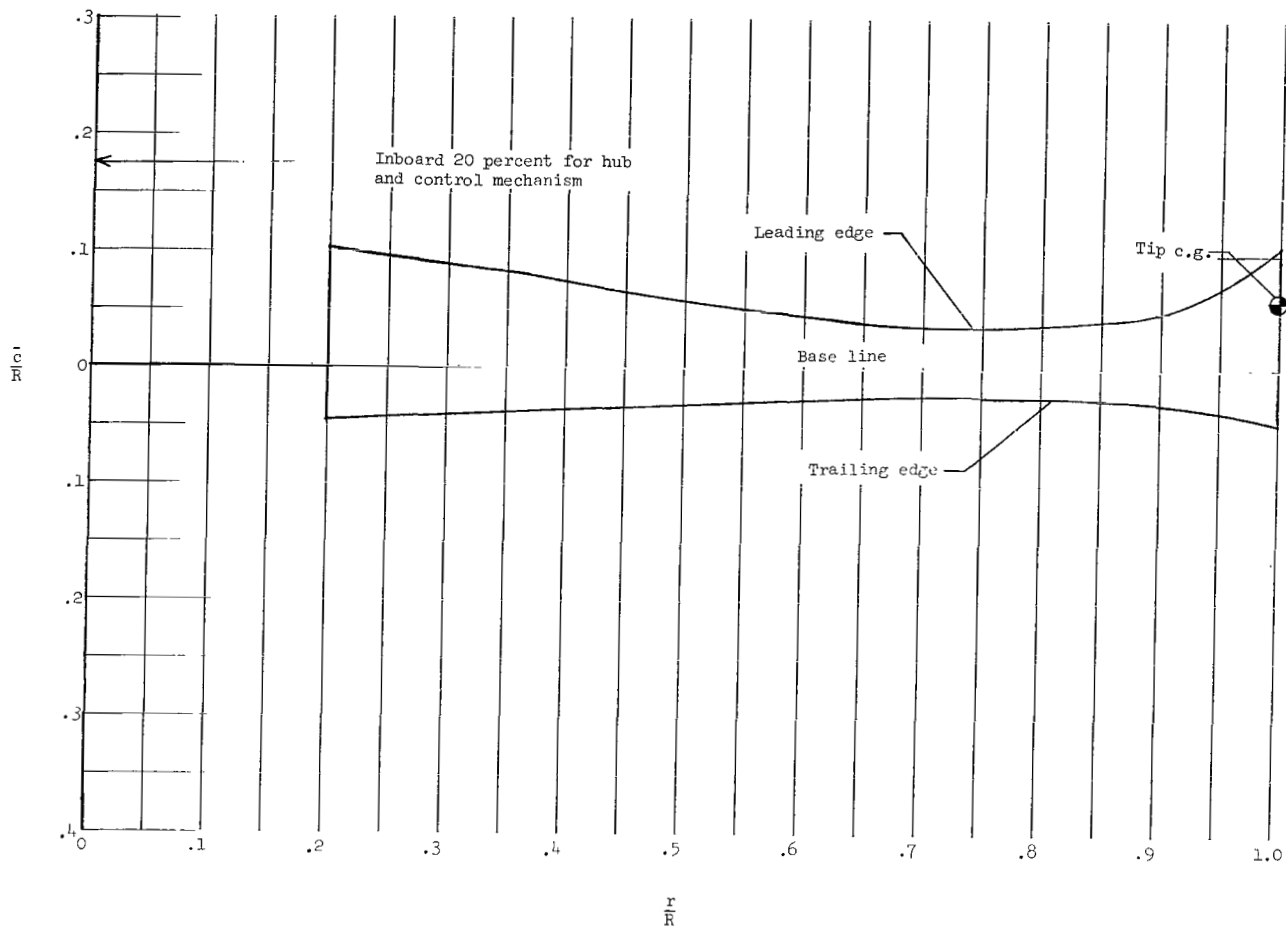


Figure 4.- Sample of calculated nonluffing platform. Radius = 20 ft (6.096 meters); tip mass = 30 lb (13.616 kilograms);  $\sigma_{tip} = 0.05$ ; minimum chord at 0.75 radius.

### Aeroelastic Stability of a Flexible Rotor

Assumptions.- For the purpose of analyzing the aeroelastic stability of a flexible rotor, a constant-chord rotor blade having chordwise stiffeners as depicted in figure 1(b) is assumed. Only the case of coupled first mode flapwise bending and torsion is considered, and flapwise and torsional displacements are assumed to be linear functions of the rotor radius.

The method of reference 3 is used in this analysis, since it applies specifically to airfoils of low torsional stiffness. This method assumes that when an unstable oscillation is encountered, the ratio of its frequency to the velocity at which it occurs is low enough that steady-state variation of lift and moment with angle of attack remains valid. Thus the analysis is believed to be compatible with projected designs for large slowly turning rotors with very high flexibility.

Analysis.- The sketch in figure 5 represents a rotor blade cross section at some radial station. The origin of coordinates is at point 0 when the half-chord point is at equilibrium. The section is displaced through a vertical distance  $y$  and an angle  $\theta$ . The center of gravity, elastic axis, and aerodynamic center, and their locations from the leading-edge point are shown as  $G$ ,  $B$ , and  $A$ , respectively.

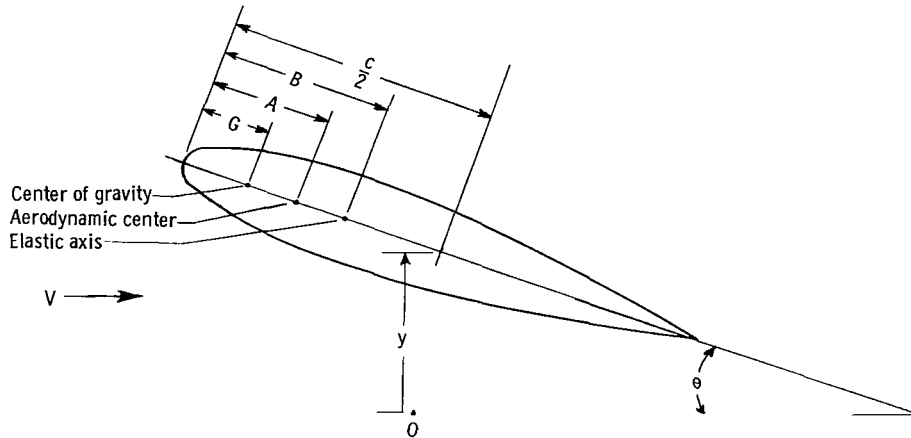


Figure 5.- Airfoil cross section.

If  $L$  is the lift per unit blade span and  $M_0$  is the moment of all aerodynamic forces about point 0, the equations of motion are as follows:

$$m \left[ \ddot{y} + \left( \frac{c}{2} - G \right) \ddot{\theta} \right] + K_y \left[ y + \left( \frac{c}{2} - B \right) \theta \right] = L \quad (7a)$$

and

$$I_G \ddot{\theta} + K_\theta \theta + K_y \left[ y + \left( \frac{c}{2} - B \right) \theta \right] (G - B) = M_0 - L \left( \frac{c}{2} - G \right) \quad (7b)$$

where  $\ddot{y}$  and  $\ddot{\theta}$  are vertical and torsional accelerations, respectively. The mass  $m$  and inertia  $I_G$  include both the airfoil and the surrounding air. The air mass is considered to be the mass of a cylinder of air of unit length with a diameter equal to the airfoil chord.

The lift per unit blade span is  $C_L \frac{1}{2} \rho V^2 c$ , and since  $C_L = a\alpha$  and  $\alpha$  is  $\theta - \dot{y}/V$  (where  $\dot{y}$  is the vertical velocity of the air relative to the blade section),

$$L = \frac{1}{2} \rho V^2 c a \left( \theta - \frac{\dot{y}}{V} \right) \quad (8a)$$

and

$$M_O = L\left(\frac{c}{2} - A\right) = \frac{1}{2} \rho V^2 c a \left(\theta - \frac{\dot{y}}{V}\right) \left(\frac{c}{2} - A\right) \quad (8b)$$

The detailed stability analysis from these equations is given in reference 3 and is not repeated herein. The important result is that the solutions define two types of aeroelastic instability: static divergence and classical flutter.

When the aerodynamic twisting moment exceeds the elastic restoring moment, the airfoil encounters a static divergence. This condition is defined when

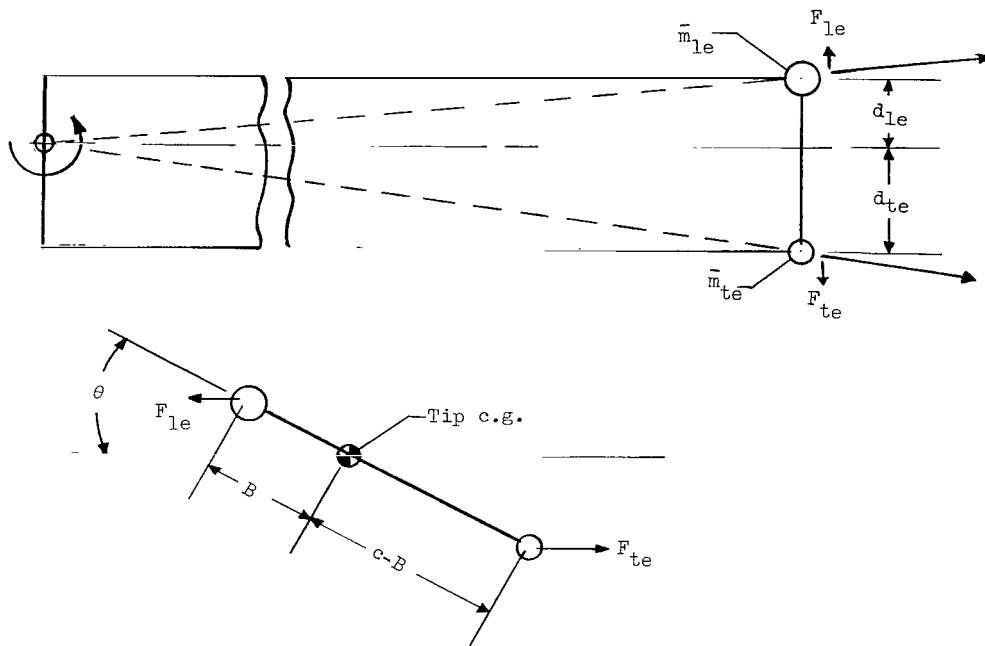
$$V^2 \geq \frac{K_\theta}{\frac{1}{2} a \rho c (B - A)} \quad (9a)$$

A true flutter occurs when

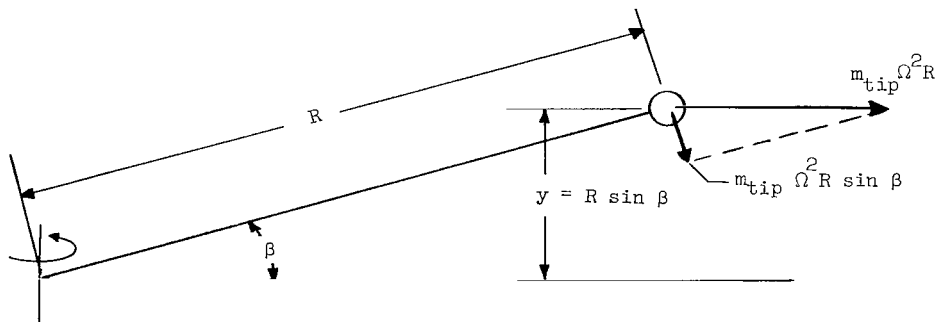
$$V^2 \geq \frac{K_\theta + K_y \left[ (G - B)^2 + \frac{I_G}{m} \right]}{\frac{1}{2} a \rho c (G - A)} \quad (9b)$$

In order to solve the foregoing stability equations, it is necessary to evaluate the spring constants  $K_y$  and  $K_\theta$  for a blade where all of the stiffness is developed by centrifugal forces. Figure 6(a) shows a rotor blade of rectangular planform with a given tip mass and tip-mass chordwise center of gravity. Because all the restraint is provided by the leading- and trailing-edge members, the elastic axis is parallel to the edges and passes through the tip-mass center of gravity. The distances  $d_{le}$  and  $d_{te}$  are functions of the rotor geometry and center of rotation. When a pure torsion is applied to the rotating blade, the restoring moment is provided by the chordwise centrifugal force components  $F_{le}$  and  $F_{te}$  acting through distances  $B \sin \theta$  and  $(c - B) \sin \theta$ , respectively. The tip body is assumed to be divided into two concentrated masses determined by the tip-body chordwise center of gravity. Therefore,

$$\left. \begin{aligned} F_{le} &= m_{tip} \left(1 - \frac{B}{c}\right) \Omega^2 d_{le} \\ F_{te} &= m_{tip} \left(\frac{B}{c}\right) \Omega^2 d_{te} \end{aligned} \right\} \quad (10a)$$



(a) Forces due to blade twist.



(b) Forces due to flapwise bending.

Figure 6.- Centrifugal spring forces on flexible blade.

The restoring moment about the center of twist  $M_\theta$  is then given as

$$M_\theta = m_{\text{tip}} \Omega^2 \sin \theta \left[ \left(1 - \frac{B}{c}\right) B d_{1e} + \frac{B}{c} (c - B) d_{te} \right] \quad (10b)$$

If  $\theta$  is assumed small,

$$\frac{M_\theta}{\theta} = K_\theta = m_{\text{tip}} \Omega^2 \left( B - \frac{B^2}{c} \right) (d_{1e} + d_{te}) \quad (10c)$$

and since  $d_{1e} + d_{te} = c$ ,

$$K_\theta = m_{\text{tip}} \Omega^2 B (c - B) \quad (10d)$$

The flapwise spring constant  $K_y$  is obtained from figure 6(b) as follows: Consider the rotating blade with tip mass moved up a distance  $y$  through an angle  $\beta$ . As previously stated, the flapwise displacement is assumed to be a linear function of the rotor radius. The force tending to rotate the blade to  $\beta = 0^\circ$  is  $m_{\text{tip}} \Omega^2 R \sin \beta$  and the distance  $y$  is  $R \sin \beta$ . Therefore, the flapwise spring constant is given as

$$K_y = \frac{m_{\text{tip}} \Omega^2 R \sin \beta}{R \sin \beta} = m_{\text{tip}} \Omega^2 \quad (11)$$

Substituting equation (10d) for  $K_\theta$  in the divergence equation (9a) yields

$$V^2 \cong \frac{m_{\text{tip}} \Omega^2 B (c - B)}{\frac{1}{2} a \rho c (B - A)} \quad (12a)$$

Equation (12a) can then be expressed as

$$V^2 \cong \left[ \frac{m_{\text{tip}} \Omega^2}{\frac{1}{2} a \rho} \right] \left[ \frac{\frac{B}{c} \left(1 - \frac{B}{c}\right)}{\frac{B}{c} - \frac{A}{c}} \right] \quad (12b)$$

Substituting for  $K_\theta$  and  $K_y$  (eqs. (10d) and (11)) in the flutter equation (9b) yields

$$V^2 \cong \left[ \frac{m_{\text{tip}} \Omega^2}{\frac{1}{2} a \rho} \right] \left[ \frac{B(c - B) + (G - B)^2 + \frac{IG}{m}}{c(G - A)} \right] \quad (13a)$$

Equation 13(a) can also be written

$$V^2 \cong \frac{\left[ \frac{m_{\text{tip}} \Omega^2}{\frac{1}{2} a \rho} \right] \left[ \frac{\frac{B}{c} \left( 1 - \frac{B}{c} \right) + \left( \frac{G}{c} - \frac{B}{c} \right)^2 + \frac{I_G}{m c^2}}{\frac{G}{c} - \frac{A}{c}} \right]}{\quad} \quad (13b)$$

The terms  $V^2$ ,  $a$ ,  $\rho$ ,  $G$ ,  $A$ , and  $I_G/m$  normally refer to blade properties at some station inboard of the tip radius since, for aeroelastic analysis of rotors, the velocity at some inboard section is considered more representative of the entire rotor. (See ref. 4.) All other terms are spring terms and refer to properties at the blade tip radius. Preliminary analysis indicated that the term  $I_G/m$  does not vary appreciably from about the three-quarter radius to the tip, and since solutions based on a blade section at the tip should be conservative, all subsequent analysis is referred to the tip radius.

The velocity  $V$  at the tip is  $\Omega R$ , and it can be shown that  $I_G/m$  at the tip is  $B(c - B)$ . Substituting for  $V$  and dividing out the first bracketed expression in equation (12b) gives

$$\frac{a \rho R^2}{2 m_{\text{tip}}} \cong \frac{\frac{B}{c} \left( 1 - \frac{B}{c} \right)}{\frac{B}{c} - \frac{A}{c}} \quad (14)$$

for the static divergence condition.

Substituting for  $V$  and  $I_G/m$  and dividing through by the first bracketed term in equation (13b) gives

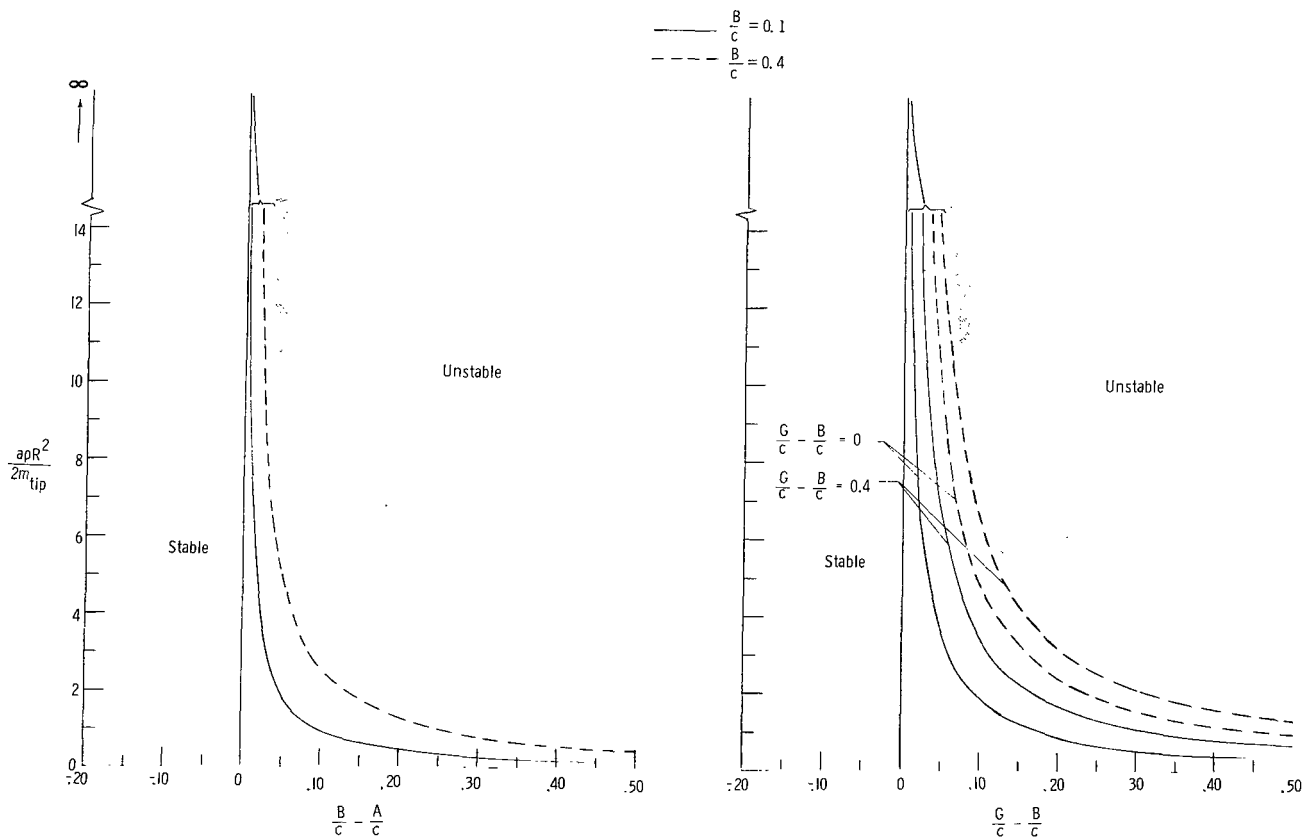
$$\frac{a \rho R^2}{2 m_{\text{tip}}} \cong \frac{2 \frac{B}{c} \left( 1 - \frac{B}{c} \right) + \left( \frac{G}{c} - \frac{B}{c} \right)^2}{\frac{G}{c} - \frac{A}{c}} \quad (15)$$

for the flutter condition.

Results. - In the foregoing analysis, the divergence and flutter boundaries of the flexible rotor have been defined as simple relationships between easily measurable rotor and blade-section properties (eqs. (14) and (15)). It should be reemphasized here that the previous analysis assumed instabilities arising from coupled bending and torsion of an airfoil with low torsional stiffness, in which the frequencies of oscillation are so low that the steady-state lift and moment variations with angle of attack remain valid. Therefore, the results are believed to be applicable to large, slowly turning rotors of extremely flexible design. One significant result is that there are no velocity terms appearing in equations (14) and (15). Therefore, as in reference 5, the conclusion can be made that

for a given hovering rotor, the aeroelastic stability is independent of the rotor rotational speed. This result, of course, ignores the effects of Mach number and compressibility.

Flexible-rotor divergence boundaries are given in figure 7(a) as the variation of a blade-mass parameter  $\frac{\rho R^2}{2m_{tip}}$  with elastic axis offset from the aerodynamic center ( $B/c - A/c$ ) for two elastic-axis positions. Flutter boundaries are given in figure 7(b) as the variation of the mass parameter with center-of-gravity offset from the aerodynamic center ( $G/c - A/c$ ) for two elastic axis positions. Two offsets between the center of gravity and the elastic axis ( $G/c - B/c$ ) are included in figure 7(b). The plots are presented in these terms since deformable blades of this type may not have fixed aerodynamic-center locations under changing conditions of operation. All points to the left of the curves represent stable combinations of blade properties, and all points to the right represent unstable combinations. Although it is always ideal to maintain both elastic axis and center of gravity forward of the aerodynamic center for conventional as well as for extremely flexible airfoils, these curves indicate the extent to which this constraint may be relaxed for the flexible type (the area bounded by the vertical axis and the given



(a) Divergence boundaries.

(b) Flutter boundaries.

Figure 7.- Aeroelastic stability boundaries for flexible rotor blades.

curves). These results are from an analysis of a constant-chord blade with chordwise stiffness; however, in the absence of luffing the results are believed to apply equally to the fully flexible type.

Extension of the aeroelastic analysis to forward-flight conditions is not attempted here, as it is believed to warrant a separate study. However, some idea of the effects of forward velocity may be obtained from the following considerations.

The previous simplifying assumptions for the hovering rotor and the additional assumption that only the forward-flight velocity increment affects the stability boundaries are made. From the previous analysis, the stability boundaries are defined by equations (12b) and (13b) as:

$$V^2 \cong \Omega^2 \left[ f_1(a, \rho, m_{\text{tip}}) f_2(A, B, c, G) \right] \quad (16)$$

where  $f_1$  and  $f_2$  denote "function of." If  $V_F$  is the forward velocity, the maximum total velocity at the advancing blade tip is  $V_F + \Omega R$ . Therefore, since the tip-speed ratio  $\mu$  is  $V_F/\Omega R$ , equation (14) (the divergence equation) can then be written as

$$\frac{a\rho R^2(\mu + 1)^2}{2m_{\text{tip}}} \cong \frac{\frac{B}{c} \left(1 - \frac{B}{c}\right)}{\frac{B}{c} - \frac{A}{c}} \quad (17)$$

Equation (15) (the flutter equation) becomes:

$$\frac{a\rho R^2(\mu + 1)^2}{2m_{\text{tip}}} \cong \frac{2 \frac{B}{c} \left(1 - \frac{B}{c}\right) + \left(\frac{G}{c} - \frac{B}{c}\right)^2}{\frac{G}{c} - \frac{A}{c}} \quad (18)$$

Equations (17) and (18) indicate that if a rotor designed for hovering according to the method outlined herein has either the center-of-gravity or elastic axis aft of the aerodynamic center, it will rapidly approach a stability boundary as forward speed is increased. One solution to this problem is to design for the maximum tip speed ratio at which a given size of rotor will operate by providing sufficient tip mass. This solution compromises the hovering performance, since added tip weight results in greater overall aircraft weight as previously discussed. Another solution is to partially retract the blade at a rate proportional to  $(\mu + 1)$ . The penalty in this case is increased disk loading in a more direct manner than in the first case. As previously stated, other factors may considerably affect the forward flight aeroelastic characteristics of extremely flexible rotors; however, the results given here suggest that the design requirements for aeroelastic stability may limit the operational envelope of a given rotor to a narrow range of forward speeds.

## EXPERIMENTAL INVESTIGATION

An experimental investigation of a fully flexible rotor has been undertaken to provide data on performance, dynamics, and operating characteristics of a rotor of this general type. A description of the rotor, test setup, and some initial results are presented in the final portion of this paper.

### Apparatus and Tests

For the experimental tests, a fully flexible rotor was used. Pertinent rotor dimensions are given in figure 8, and a photograph of the rotor mounted on the Langley helicopter test tower is presented as figure 9.

The leading and trailing edges of the blades are very high strength steel rods, and the fabric airfoil is low porosity dacron sailcloth. The tip body is steel and aluminum, and the tip body stabilizer is a swept ( $30^\circ$ ) NACA 0006 aluminum airfoil the incidence of which was set at  $-10^\circ$  with respect to the tip-body chord plane. The chordwise center of gravity of the tip body was set at 25 percent of the blade tip chord from the leading edge. The rotor was driven from the tower drive system through a range of tip speeds up to 320 feet per second (97.54 meters per second). Forces and moments, control positions, vibrations, and rotor speed were remotely indicated. The sensors on one blade were fed into a recording oscillograph and sensors on the other blade were fed into microammeters and monitored during the tests. The output of a vibration pickup mounted on the tower structure was monitored and used as the primary indication of limiting conditions for operation. A rotating motion-picture camera mounted on the rotor hub was used to record the behavior of one blade during operation.

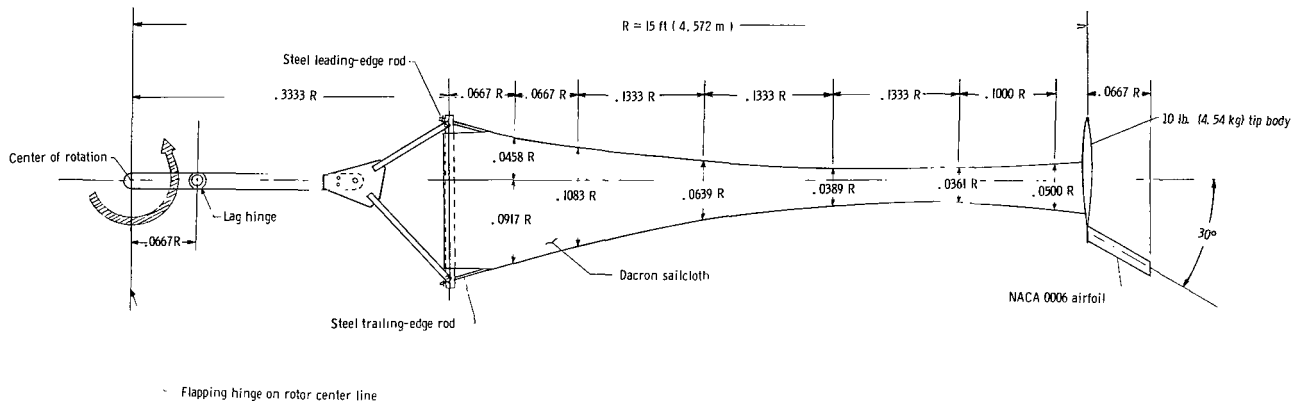


Figure 8.- Principal dimensions of experimental flexible rotor.



Figure 9.- Experimental rotor mounted on Langley helicopter test tower.

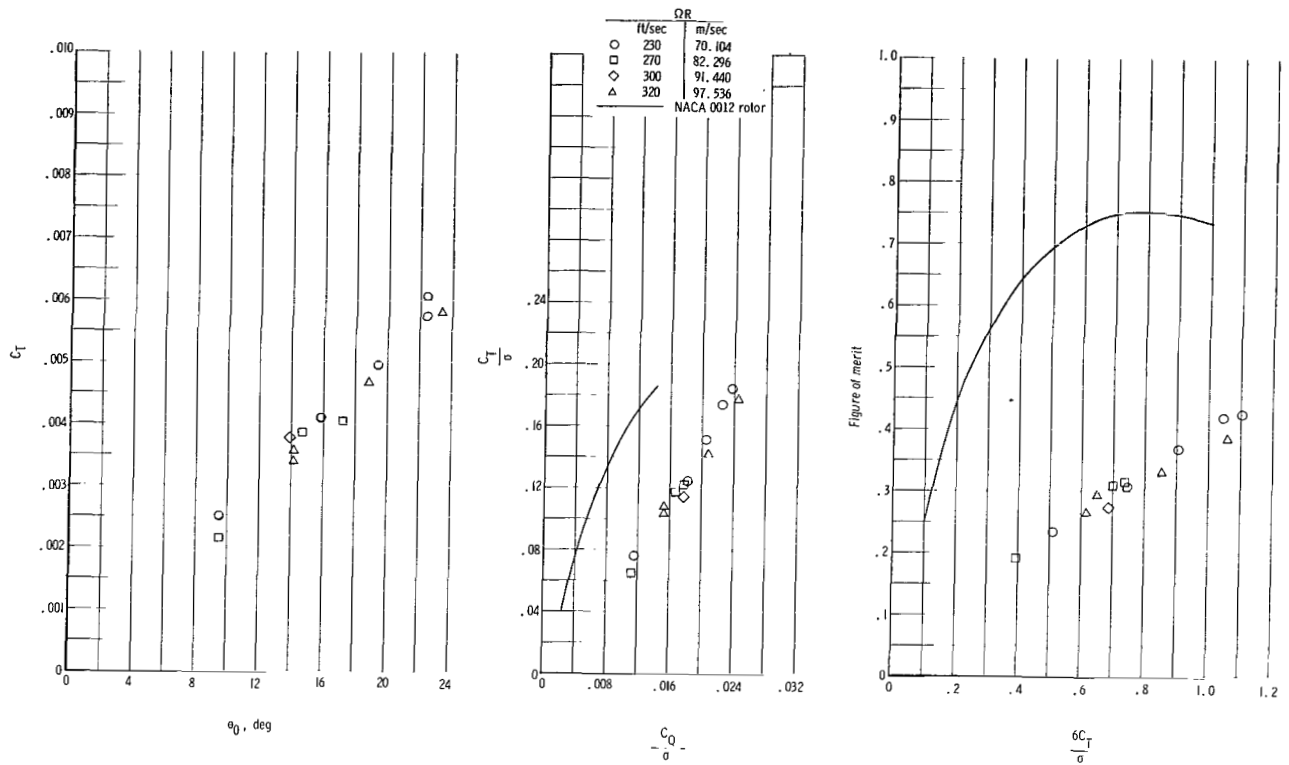
L-68-811

Measurements were made through a tip speed range at several angles of collective pitch at the blade root for a fixed tip body center of gravity (25 percent chord) and a  $-10^{\circ}$  tip stabilizer incidence.

### Results

Stability.- The range of conditions through which measurements were made was dictated by the level of vibration judged to be within structurally safe limits. The source of these vibrations was fabric instability (considered to be luffing) that occurred at low pitch angles and blade stall that occurred at high pitch angles. The vibrations at low pitch angles were considered to be luffing since at a given rotor speed, they could usually be diminished by increasing the blade pitch. Also, when the test rotor was analyzed according to equation (6c), the results indicate that the tip mass was about 30 percent less than that required for a nonluffing rotor. Unfortunately, the aeroelastic stability of the rotor can not be estimated from figure 7. Neither the lift-curve slopes of the various airfoil shapes generated during operation, nor the aerodynamic-center location and its sensitivity to changing conditions is known. These factors must be determined from two-dimensional tests of flexible airfoils before the behavior of flexible rotor blades of this type can be fully understood.

Performance.- The hovering characteristics of one configuration of the test rotor are given in figure 10. The variation of thrust coefficient with blade-root pitch angle  $\theta_0$



(a) Variation of thrust coefficient with collective pitch angle at blade root.

(b) Variation of thrust coefficient-solidity ratio with torque coefficient-solidity ratio.

(c) Variation of rotor figure of merit with rotor mean lift coefficient  $6C_T/\sigma$ .

Figure 10.- Hovering performance characteristics of flexible rotor configuration. Tip stabilizer incidence =  $-10.0^\circ$ ; 10 lb (4.54 kg) tip body.

(fig. 10(a)) shows that the overall rotor thrust continued to increase in the range where vibrational levels indicate severe stall. Because of the nature of the blade response to root pitch inputs, however, the blade twist is high at these conditions, and the outboard portions of the blade (which provide the greatest percentage of the thrust) remain unstalled.

The variation of the ratio of thrust coefficient to solidity with the ratio of torque coefficient to solidity is given in figure 10(b), and the variation of rotor figure of merit with rotor mean lift coefficient is given in figure 10(c). Curves for a conventional rotor with NACA 0012 airfoil sections (ref. 6) are included for comparison. The flexible rotor had considerably higher power consumption and lower efficiency than the 0012 rotor as shown in figure 10(b). This result is indicative of high profile drag from blade deformations and excessive twist. Although the flexible-rotor figure of merit was considerably lower than that of the conventional rotor for the range of test conditions (fig. 10(c)), the

flexible rotor attained mean lift coefficients in excess of 1.0 prior to any indication of stall. These high mean lift coefficients are a result of the blade section camber developed in operation.

The test results suggest that some means of controlling the blade twist, and modification of the spanwise area distribution or both would provide significant benefits in terms of better hovering efficiency. Further experiments are necessary to determine the relative effects of tip stabilizer setting, tip body center of gravity, and other blade parameters in efforts to obtain a more general understanding of flexible rotor behavior.

## CONCLUSIONS

From the results of an analytical and experimental investigation of extremely flexible rotors, the following points are concluded:

1. Of the two types of flexible rotors considered (fully flexible and rigid chord), the fully flexible type appears least promising. Its operational range in terms of speed and blade pitch may be severely limited by luffing (fabric instability). Analysis indicates that careful design of this type of rotor is necessary to insure compatibility of tip mass and blade planform in order to avoid this phenomenon.

2. The tip mass requirements for a nonluffing, fully flexible rotor blade indicate that large rotors of this type may sacrifice the expected performance benefits of low disk loading.

3. Provision of some degree of chordwise stiffness is expected to result in an improved flexible rotor design for hovering. Tip mass requirements should not be severe, and large rotors of this type are more likely to accrue the benefits of low disk loadings. Rotor blade geometry is not dictated by the requirements for avoidance of luffing, and thus designs can be based on more important performance considerations such as solidity and planform taper.

4. An elementary aeroelastic analysis of a rigid-chord flexible rotor in hover indicates that the aeroelastic stability is independent of rotational speed. The results also indicate the extent to which the usual design constraint (complete mass balance about the aerodynamic center for stability at any speed) may be relaxed in the design of flexible rotors.

5. Preliminary results from a hovering investigation of a fully flexible rotor indicate high power consumption, low efficiency, and high mean lift coefficients for the particular configuration tested. The high power consumption and low efficiency are attributed to the blade deformations and excessive blade twist peculiar to this particular rotor

design. The high mean lift coefficients are attributed to the large amounts of blade camber induced aerodynamically during operation.

Langley Research Center,  
National Aeronautics and Space Administration,  
Langley Station, Hampton, Va., November 20, 1967,  
721-01-00-28-23.

## APPENDIX

### NUMERICAL EXAMPLE OF NONLUFFING FLEXIBLE ROTOR PLANFORM

This appendix contains a numerical example of a nonluffing flexible rotor planform calculated according to the method outlined in the main body of this paper. This illustration is intended to apply to hovering conditions only.

The following values are assumed to be known:

Rotor radius, $R$ . . . . .	20 ft (6.096 meters)
Tension constant, $K_t$ (from ref. 2, $K_t > 1.73$ ) . . . . .	2.0
Tip solidity, $\sigma_{tip}$ . . . . .	0.05
Radius ratio to minimum chord, $x_0$ . . . . .	0.75
Tip-body center of gravity . . . . .	0.25c
Air density, $\rho$ . . . . .	0.002378 slugs/ft <sup>3</sup> (1.226 kg/meter <sup>3</sup> )

From the value  $\sigma_{tip} = 0.05$ ,

$$c_{tip} = 0.05\pi R = 3.14 \text{ ft (0.957 meter)}$$

From the condition  $m_{tip} > \frac{1}{2} K_t \rho R^2 c_{tip} (1 - x_0)$

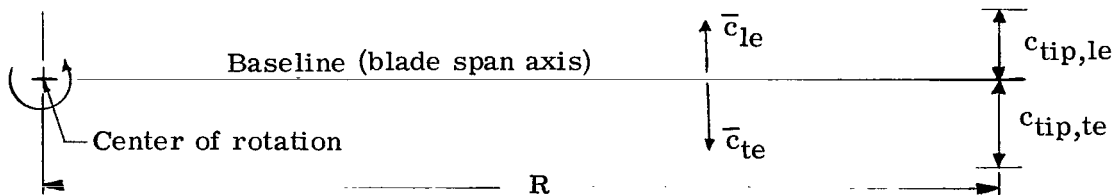
$$m_{tip} > 0.747 \text{ slug (10.902 kilograms)}$$

Let  $m_{tip} = 30 \text{ lbm}$  or  $0.932 \text{ slug}$  (13.602 kilograms). Then from the tip center-of-gravity condition,

$$\bar{m}_{le} = 0.75 \times 0.932 = 0.699 \text{ slug (10.201 kilograms)}$$

$$\bar{m}_{te} = 0.25 \times 0.932 = 0.233 \text{ slug (3.400 kilograms)}$$

The following diagram indicates the positions of various rotor parameters:



## APPENDIX

The chord is then determined at the blade tip as

$$\bar{c}_{tip,le} < \frac{\bar{m}_{1e}}{\frac{1}{2} K_t \rho R^2 (1 - x_o)}$$

$$\bar{c}_{tip,le} < 2.935 \text{ ft (0.895 meter)}$$

$$\bar{c}_{tip,te} < \frac{\bar{m}_{te}}{\frac{1}{2} K_t \rho R^2 (1 - x_o)}$$

$$\bar{c}_{tip,te} < 0.980 \text{ ft (0.299 meter)}$$

Therefore, let

$$c_{tip,le} = 2.20 \text{ ft (0.671 meter)}$$

and

$$c_{tip,te} = 0.94 \text{ ft (0.287 meter)}$$

These dimensions are measured normal to a base line as shown in the preceding sketch. With conditions fixed at the blade tip, chord values at successive stations along the blade can be computed from:

$$\log_e \bar{c} = \frac{K_t \rho R^3}{24} \left\{ \frac{3(x^4 - 1) + x_o(1 - x^3)}{\left[ \bar{m}^2 - \left[ \frac{1}{2} K_t \rho R^2 \bar{c}_{tip} (1 - x_o) \right]^2 \right]^{1/2}} \right\} + \log_e \bar{c}_{tip}$$

Figure 4 is a plot of a computed planform of a rotor with the properties given in this appendix.

## REFERENCES

1. Mechtly, E. A.: The International System of Units – Physical Constants and Conversion Factors. NASA SP-7012, 1964.
2. Nielsen, Jack N.: Theory of Flexible Aerodynamic Surfaces. Trans. ASME, Ser. E: J. Appl. Mech., vol. 85, no. 3, Sept. 1963, pp. 435-442.
3. Den Hartog, J. P.: Mechanical Vibrations, Fourth ed., McGraw-Hill Book Co., Inc., 1956.
4. Brooks, George W.; and Baker, John E.: An Experimental Investigation of the Effect of Various Parameters Including Tip Mach Number on the Flutter of Some Model Helicopter Rotor Blades. NACA TN 4005, 1958. (Supersedes NACA RM L53D24.)
5. Goldman, Robert L.: Some Observations on the Dynamic Behavior of Extremely Flexible Rotor Blades. Paper No. 60-44, Inst. Aero. Sci., Jan. 1960.
6. Carpenter, Paul J.: Lift and Profile-Drag Characteristics of an NACA 0012 Airfoil Section as Derived From Measured Helicopter-Rotor Hovering Performance. NACA TN 4357, 1958.

National Aeronautics and Space Administration  
WASHINGTON, D. C.  
OFFICIAL BUSINESS

FIRST CLASS MAIL

POSTAGE AND FEES PAID  
NATIONAL AERONAUTICS AND  
SPACE ADMINISTRATION

070 001 26 51 3DS 68074 00403  
AIR FORCE WEAPONS LABORATORY/AFWL/  
KIRTLAND AIR FORCE BASE, NEW MEXICO 87117

ATTN: MISS ADELINE F. CANOVA, CHIEF TECHNIC  
LIBRARY 76117

POSTMASTER: If Undeliverable (Section 15  
Postal Manual) Do Not Return

*"The aeronautical and space activities of the United States shall be conducted so as to contribute . . . to the expansion of human knowledge of phenomena in the atmosphere and space. The Administration shall provide for the widest practicable and appropriate dissemination of information concerning its activities and the results thereof."*

—NATIONAL AERONAUTICS AND SPACE ACT OF 1958

## NASA SCIENTIFIC AND TECHNICAL PUBLICATIONS

**TECHNICAL REPORTS:** Scientific and technical information considered important, complete, and a lasting contribution to existing knowledge.

**TECHNICAL NOTES:** Information less broad in scope but nevertheless of importance as a contribution to existing knowledge.

**TECHNICAL MEMORANDUMS:** Information receiving limited distribution because of preliminary data, security classification, or other reasons.

**CONTRACTOR REPORTS:** Scientific and technical information generated under a NASA contract or grant and considered an important contribution to existing knowledge.

**TECHNICAL TRANSLATIONS:** Information published in a foreign language considered to merit NASA distribution in English.

**SPECIAL PUBLICATIONS:** Information derived from or of value to NASA activities. Publications include conference proceedings, monographs, data compilations, handbooks, sourcebooks, and special bibliographies.

**TECHNOLOGY UTILIZATION PUBLICATIONS:** Information on technology used by NASA that may be of particular interest in commercial and other non-aerospace applications. Publications include Tech Briefs, Technology Utilization Reports and Notes, and Technology Surveys.

*Details on the availability of these publications may be obtained from:*

SCIENTIFIC AND TECHNICAL INFORMATION DIVISION  
NATIONAL AERONAUTICS AND SPACE ADMINISTRATION

Washington, D.C. 20546